2c 6
Copy
RM E54C08

NACA RM E54C08

RESEARCH MEMORANDUM

EVALUATION AT SUPERSONIC SPEEDS OF TWIN-DUCT SIDE-INTAKE SYSTEM WITH TWO-DIMENSIONAL DOUBLE-SHOCK INLETS

By Leonard J. Obery, Leonard E. Stitt, and George A. Wise

Lewis Flight Propulsion Laboratory
Cleveland, Ohio

NATIONAL ADVISORY COMMITTEE
FOR AERONAUTICS

WASHINGTON

August 19, 1954

NACA RM E54C08

NATIONAL ADVISORY COMMITTEE FOR AERONAUTICS

RESEARCH MEMORANDUM

EVALUATION AT SUPERSONIC SPEEDS OF TWIN-DUCT SIDE-INTAKE SYSTEM WITH TWO-DIMENSIONAL DOUBLE-SHOCK INLETS

By Leonard J. Obery, Leonard E. Stitt,
and George A. Wise

SUMMARY

The performance of a twin-duct air-intake system utilizing a double-oblique-shock inlet with a variable second ramp was investigated in the Lewis 8- by 6-foot supersonic tunnel at free-stream Mach numbers of 0.62, 1.5, 1.8, and 2.0. The test was conducted over a range of angles of attack and yaw, mass-flow ratio, and variable-ramp angle. In contrast with the behavior of a similar duct system utilizing single-shock fixed inlets, dissimilar operation of the twin ducts occurred at the supersonic Mach numbers in that one duct operated supercritically while the other was subcritical. The stable subcritical range at Mach numbers 1.8 and 2.0 decreased as the variable-ramp angle decreased. Experimental total-pressure recovery of 85 percent was obtained at a free-stream Mach number of 2.0. Included in this 15 percent loss is a 4 percent loss of free-stream total pressure ahead of the inlet caused by the fuselage forebody. At a free-stream Mach number of 0.62 good agreement was realized between experimental and theoretical total-pressure recovery for sharp-lip inlets. The variable-ramp inlet enabled the engine to be matched to the inlet at a high pressure recovery throughout the supersonic Mach number range.

INTRODUCTION

An investigation has been conducted in the 8- by 6-foot supersonic tunnel of the NACA Lewis laboratory to evaluate the internal and external performance of several twin-duct air intake systems mounted on the sides of a supersonic aircraft. The performance characteristics of several single-oblique-shock inlets designed for a J57 engine were reported in references 1 and 2. To extend the flight Mach number range of the prototype, the J57 engine will be replaced with a J67 engine.

Because of the extended Mach number range, a fixed-geometry inlet was not considered satisfactory. Therefore, an inlet incorporating a

variable-angle ramp was designed to provide the required air flow to the engine at a high pressure recovery and a low inlet drag throughout the Mach number range. The boundary-layer splitter plate, located immediately ahead of the variable-angle ramp, was formed into a precompression wedge to increase the efficiency of the external compression of the entering stream tube. This report concerns the evaluation of the double-oblique-shock inlet system designed for the higher Mach number configuration.

The investigation was conducted over a range of angle of attack and yaw at free-stream Mach numbers M_0 of 2.0, 1.8, 1.5, and 0.62.

SYMBOLS

The following symbols are used in this report:

A	area
C_D	external drag coefficient based on maximum frontal cross-sectional area of 2.09 sq ft, D/q_0A_f
$C_{T,B}$	boundary-layer bleed-duct thrust coefficient based on maximum frontal cross-sectional area of 2.09 sq ft
D	drag
F_n	engine thrust at diffuser total-pressure recovery
$F_{n,id}$	engine thrust at 100 percent diffuser total-pressure recovery
L	length of subsonic diffuser, 81.5 in.
M	Mach number
m_B/m_0	boundary-layer bleed-duct mass-flow ratio, boundary-layer mass flow/$\rho_0V_0A_{i,B}$
m_3/m_0	engine mass-flow ratio, engine mass flow/$\rho_0V_0A_i$
m*	reference mass flow, value corresponding to choking (M = 1.0) at inlet throat area at free-stream total pressure
P	total pressure
p	static pressure
q	dynamic pressure, $\gamma pM^2/2$

T	total temperature
V	velocity
W	air flow
x	distance from cowl lip, model station 36
α	model angle of attack
γ	specific heat, 1.4
δ	P/2116
θ	T/519
λ	angle of variable ramp with respect to fuselage center line, deg
ρ	mass density of air
ψ	model angle of yaw

Subscripts:

B	boundary-layer bleed-duct-exit survey station, model station 101.25
x	conditions at x-distance from cowl lip
0	free stream
1	fuselage survey station, model station 31
2	diffuser-inlet survey station, model station 40
3	diffuser-exit survey station, model station 100

Pertinent areas:

A_f	maximum frontal cross-sectional area, 2.09 sq ft
A_i	projected frontal area of both inlets, 0.36 sq ft
$A_{i,B}$	inlet area of one boundary-layer bleed duct, 0.00936 sq ft
A_3	flow area at diffuser discharge, 0.457 sq ft

[redacted]

APPARATUS AND PROCEDURE

The model investigated is illustrated photographically in figure 1 and schematically in figure 2. Shown in these figures are the twin double-ramp side inlets mounted on the 1/4-scale fuselage forebody of a supersonic airplane. The ducts were geometrically similar and joined into a common duct at a model station which corresponded to the engine compressor face in the prototype.

The model was sting-mounted in the tunnel through a system of strain-gage balances. The dark extension to the fuselage, which can be seen in figure 1, was a shroud used to protect various mechanisms. It was also attached to the sting but was entirely independent of the model. The reverse scoop seen in figure 1 was one of two mounted on the shroud to lower the pressure at the base of the model and insure choking at the mass-flow control plugs.

Details of the model, including internal flow stations and representative model cross sections, are shown in figure 2. The nose of the model was canted down at an angle of 5°, and the inlets were canted at an angle of 3°, both with respect to the fuselage center line. The 5° droop of the nose was intended to facilitate pilot vision in the prototype rather than to influence flow conditions for maximum performance.

A photograph and a schematic drawing of the inlet are presented in figures 3 and 4, respectively. The inlet had a fixed 10° precompression ramp with the leading edge positioned so that the resulting oblique shock was located just ahead of the cowl lip at a Mach number of 2.0. The first ramp also acted as a boundary-layer splitter plate and was sufficiently distant from the fuselage to effect complete removal of the body boundary layer. The second ramp was hinged at its leading edge to the first ramp and was remotely variable through an angle range from 0° to 22° with respect to the fuselage center line (fig. 4(c)). Changes in the second ramp angle varied the cross-sectional area distribution of the initial part of the subsonic diffuser, as is shown in figure 5 for several ramp angles.

Boundary-layer removal was effected through the use of ram-type boundary-layer scoops (fig. 4(b)) located beneath the center portion of the inlet ramps. The boundary-layer ducts, which changed smoothly from a rectangular cross section at the inlet to a circular cross section, discharged the boundary-layer air at the exit station in a direction parallel to the main duct. Boundary-layer mass flows were varied by means of remote-controlled plugs (fig. 2). The air in excess of that passing through the bleed ducts was spilled out the open sides of the scoop by wedges, as shown in figure 4(b).

Both of the main ducts were instrumented at model station 40 with total-pressure rakes (fig. 3) and wall static-pressure orifices, one located at the base of each rake. The rakes were used to obtain the total-pressure recovery across the face of the inlet. At model station 100, the main duct was instrumented with six equally spaced total pressure rakes of four tubes each with a static-pressure orifice at the ends of each rake. Immediately downstream of these rakes, at model station 107, were located eight static-pressure orifices, four in the centerbody and four on the duct wall. Mass-flow calculations were made using the average static pressure obtained from these orifices with the assumption that the flow was choked at the geometric minimum area determined by the exit plug. Mass-flow ratio m_3/m_0 is defined as the ratio of the mass flow through the diffuser ducts to the mass flowing in the free stream through an area equal to the total inlet projected area.

One of the boundary-layer ducts was instrumented with two static-pressure orifices at the inlet, and with four static-pressure orifices and a five-tube total-pressure rake at the exit. Mass-flow ratios were calculated from the static- and total-pressure measurements at the exit and were referenced to the bleed-duct inlet area. The boundary-layer duct force was calculated for the range of mass-flow ratios as the change in total momentum from the bleed inlet to the bleed exit. The duct force resulted from the action of the bleed plugs and was inherent in the manner of testing.

Forces on the model were measured with an internal strain-gage balance located at a forward station in the model and a double-link strain-gage unit mounted between the rear model bulkhead and the sting. The rear link measured a normal component of force only and additionally restrained the model in pitch. The rear link therefore prevented most of the model deflection due to imposed air loads. Forces measured by the balance system were the combined internal duct forces, fuselage drag, and base force. The drag presented is the streamwise component of the external forces, excluding the base pressure force and the stream thrust developed by the main duct flow from free-stream to exit. Included in the drag is the momentum change due to the flow through the boundary-layer ducts; however, during the test the mass-flow control plugs were set at a position corresponding to approximately zero boundary-layer duct force.

The test was conducted at free-stream Mach numbers of 0.62, 1.5, 1.8, and 2.0, at various angles of attack and yaw, and for a range of mass-flow ratios. The Reynolds number based on the length of the fuselage ahead of the inlets was 13×10^6.

RESULTS AND DISCUSSION

The performance characteristics of the inlet and ducting system at $M_0 = 2.0$ are presented in figure 6 for the variable ramp set at 19°. Shown on the internal performance curves are lines of constant corrected weight flow, a particular one being labeled "Match line" which corresponds to the corrected weight flow required by the J67-W-1 engine at 35,000 feet altitude. The total-pressure-recovery curves for $M_0 = 2.0$ indicate that peak recovery of approximately 85 percent was obtained at angles of attack from $3\frac{1}{2}^\circ$ to 5°. At $3\frac{1}{2}^\circ$, previous measurements indicated that the inlet would be nearly alined with the local flow, and at 5° the nose was alined with the free-stream flow. As contrasted with the data of references 1 and 2, positive angles of attack greater than 5° reduced the internal performance markedly, probably because of the higher local flow angle sustained by the present inlet resulting from its lesser cant. Also because of the local flow angularity, the negative angle of attack performance was adversely affected. At $M_0 = 2.0$, the peak total-pressure recovery was considerably lower than might be expected from a double-shock inlet because of a 4 percent loss in total-pressure recovery ahead of the inlet due to the airplane forebody. It is believed that the points of highest mass-flow ratio in figure 6 nearly represent the maximum mass-flow ratio for the twin-duct system. As indicated by the curves, this maximum mass-flow ratio was only about 2 percent lower than theoretically expected.

As in reference 1, the minimum drag occurred between angles of attack of $3\frac{1}{2}^\circ$ and 5°, although this trend is barely distinguishable at $M_0 = 2.0$ because of the closeness of the data. The drag rise due to subcritical operation was approximately the same for all angles of attack and was about the magnitude that would be calculated from various theories.

Decreasing the variable-ramp angle caused relatively small changes in the peak total-pressure recovery but increased the maximum capture mass-flow ratio considerably, as shown in figure 7. Theoretically, the supersonic total-pressure recovery decreases with decreasing variable-ramp angle. However, it is believed that the decrease in supersonic recovery at the lower ramp angles was compensated by an increase in subsonic diffuser recovery caused by the lower inlet Mach number. The stable subcritical range progressively decreased from approximately 13 percent at the highest ramp angle to about 6 percent at the lowest ramp angle tested. The approximate pressure recovery level during unstable flow at the lower mass-flow ratios is shown as a dashed curve for $\lambda = 19^\circ$. The inlet match point, or the point at which the inlet would operate when coupled with the J67-W-1 engine, moved to a higher total-pressure recovery - mass-flow ratio level as the ramp angle was

decreased from 20° to 17°, as shown by the intersection of the match line with the various performance curves. Although $\lambda = 17^\circ$ would appear to be the most desirable operating condition, it is apparent that a very limited stable subcritical range is available at this ramp setting. Practical considerations, then, such as differences in weight flow between production engines, would probably indicate a selection of the more conservative 18° or 19° ramp angle. It is also evident that matching would be based almost entirely on internal performance, since the data show only slight changes in drag at the match condition for the various ramp settings.

Similar performance characteristics were obtained at $M_0 = 1.8$, as shown in figure 8, except that data for supercritical flow in both ducts were obtained as indicated by the constant mass flow portion of the performance curves. Decreasing the ramp angle from 18° to 14° showed only slight differences in peak pressure recovery but large increases in maximum capture mass-flow ratio because of the rotation of the variable-ramp oblique shock. The increased mass-flow ratio and pressure recovery at the lower ramp angles indicate that matching would be better at those values of λ, as shown by the intersection of the match line with the performance curves. However, the inlet stability decreases at the lower angles, and again inlet stability considerations would probably indicate the use of $\lambda = 16^\circ$ even though best performance would not be obtained. As before, only small changes occurred in the forebody drag at the match conditions with changes in ramp angle, and matching considerations would therefore be based primarily on internal performance.

At Mach number 1.5, the precompression wedge angle was nearly the maximum allowable for shock attachment; therefore the variable ramp was also positioned at 10° and, effectively, the inlet operated with only one compression wedge. The peak total-pressure recovery of the inlet (fig. 9) was approximately the same as that of the 9° inlet of reference 2, and the minimum forebody drag was slightly higher than that of the inlet of reference 2. The drag rise due to subcritical operation is of approximately the magnitude predicted from various theories. Comparison with the data of reference 2 indicates that the drag rise of the present model was approximately twice the magnitude of that of the previous test.

Contours of total-pressure recovery at the inlet (station 2) and at the diffuser exit (station 3) are presented in figure 10 for various model conditions at the supersonic free-stream Mach numbers. Figure 10(a) shows the inlet and exit flow for a subcritical mass-flow ratio at Mach number 2.0. The inlet contours for both ducts indicate a region of low total-pressure recovery flow near the cowl wall of about the value expected from normal shock recovery following an initial 10° compression. Near the center of the duct, the total-pressure recovery is approximately that expected from the two-wedge system followed by a

normal shock, considering in both cases that approximately 4 percent of the free-stream total pressure was lost ahead of the inlet. It thus may be concluded that two distinct regions of flow exist in the duct; one produced by external compression from the 10° ramp only and the second from the external compression of both wedges. A rather large boundary layer on the ramp surface is also apparent, especially near the center of the ramp wall. Both the inlet and exit contours indicate somewhat more flow through the right duct than the left, as evidenced by the higher total-pressure recoveries in the right duct.

A more noticeable difference in the twin duct operation is shown in figure 10(b). At this condition, the shock pattern in the right duct has changed to eliminate the low compression region, while in the left duct it is still apparent. Comparison of figures 10(b) and 10(c) indicates that no further change occurs in the right duct. Thus it may be concluded that the right duct is operating critically or supercritically for these conditions, whereas the left duct is still operating subcritically at the mass-flow ratio of figure 10(b). The diffuser-exit contours of figure 10(c) together with the performance curves of figure 6 indicate that the left duct does not become critical until the inlet system has suffered considerable total-pressure losses. It can also be seen that the exit contours indicate unequal flow until this operating condition is reached. These differences in duct flow probably result from minor but significant differences in the area variation in the duct and possibly from differences in the amount of deflection of the movable ramp and adjoining back plates.

This dissimilar flow condition is also apparent at $\alpha = 10°$, as evidenced by the contours of figure 10(d). Low compression flow regions exist near the top of both ducts near the cowl walls. Regions of separated flow, evident near the ramp wall at the bottom of the inlet, result from the local flow angle over the inlet side fairings. These inlet flow conditions persist back to the diffuser exit where higher total-pressure recoveries, and hence more mass flow, are shown on the right side of the duct than on the left and regions of higher total-pressure recovery are located near the top half of the duct. At negative angles of attack (fig. 10(e)) flow conditions similar to those at $\alpha = 10°$ exist, except that the top portion of the inlet is now subjected to leeward flow producing separated regions. The low compression flow region is evident in the lower half of the left inlet. The diffuser-exit contour indicates flow patterns corresponding to the inlet flow conditions shown.

At a Mach number of 1.8 (figs. 10(f) and 10(g)) the dissimilar operation of the twin ducts is again evident as it was at $M_0 = 2.0$. However, the left duct now is carrying a higher mass flow and reaches critical flow sooner than the right duct, as shown in figure 10(g). Therefore, the dissimilar operation of the twin ducts is probably a

function of ramp and plate deflections or of velocity perturbations ahead of the inlets rather than of differences in the fixed portion of the inlet system. Inasmuch as equal flows were obtained in the twin ducts of references 1 and 2, it is believed that tunnel conditions did not cause the dissimilar operation.

At $M_0 = 1.5$ for $\lambda = 10^\circ$, the distinct regions of flow compression would not be expected because of the elimination of the second oblique shock. As shown in figure 10(h) for a slightly subcritical operating condition, uniform flow existed over most of the inlet for both ducts; however, relatively thick boundary layers are evident on the ramp wall. At the low mass-flow-ratio condition, as shown in figure 10(i), the left duct is taking the larger share of the total mass flow with a region of separated air near the right duct ramp. The same type flow was also noted at the lower mass-flow ratios for the inlet in reference 1. This condition also exists at the diffuser-exit station with higher total-pressure recoveries evident on the left duct side of the diffuser exit and, correspondingly, with more mass flow in that area.

3229

CD-2

The breakdown of total-pressure-ratio losses is presented in figure 11 for the supersonic Mach numbers investigated at an angle of attack of 3.5°. The estimated values of subsonic diffuser losses were calculated using an adaptation of the method of reference 3. At the mass-flow ratio at which one duct becomes critical, the curves indicate that for M_0 of 2.0 the supersonic losses $\Delta P_{1-2}/P_0$ are approximately 4 percent larger than expected from shock losses. As shown by the contours of inlet total-pressure recovery for M_0 of 2.0 (fig. 10(b)), the regions of low total-pressure recovery at the cowl wall of the left duct and the rather thick boundary layer on the ramp surface of both ducts accounted for the difference between estimated and experimental supersonic losses. The experimental supersonic losses for double-shock external compression across the inlet as determined from figure 10(c), however, are only about 2 percent greater than would be expected. The experimental values of total-pressure-ratio loss ahead of the inlet $\Delta P_{0-1}/P_0$ were obtained from unpublished results of a previous investigation having the same model nose configuration. At M_0 of 1.8, the experimental supersonic losses were approximately $2\frac{1}{2}$ percent greater than estimated, again because of the low compression region in one duct and the thick boundary layer on the surface of the inlet ramps. For critical flow at M_0 of 1.5, the experimental supersonic losses were $1\frac{1}{2}$ percent greater than the estimated value. The inlet contours (fig. 10(h)) show that the theoretical recovery was attained over a large part of the inlet but also indicate a rather thick boundary layer near the ramp surface, accounting for the difference between experimental and estimated supersonic recovery. The subsonic

diffuser total-pressure-ratio loss $\Delta P_{2-3}/P_0$ at critical flow for M_0 of 1.5 was $2\frac{1}{2}$ percent less than estimated, with the result that the experimental value of total-pressure recovery agreed very closely with the estimated value. The increase in supersonic loss in the low subcritical region for M_0 of 1.5 resulted from the thick ramp boundary layer and a region of separated air near the ramp surface of the right duct, as indicated by the inlet contours shown in figure 10(i).

The internal performance and the diffuser-exit total-pressure-recovery contours of the inlet over a range of yaw angle and mass-flow ratio are presented in figures 12 and 13, respectively, for free-stream Mach numbers of 2.0, 1.8, and 1.5. The performance throughout the yaw range was obtained with the body at zero angle of attack and consequently with an inlet angle of attack of -3°. Figure 12 indicates a reduction in critical total-pressure recovery and stable mass-flow range with increasing angle of yaw. Dissimilar duct operation was observed at all yaw angles. Diffuser-exit total-pressure-recovery contours (fig. 13) indicate more mass flow through the windward duct and higher total-pressure recovery in the corresponding half of the diffuser exit than obtained in the leeward duct with increasing yaw angle.

The internal performance of the inlet at a free-stream Mach number of 0.62 is presented in figure 14 over a range of mass-flow ratio at several angles of attack for the variable-ramp angle set at 0°, as indicated in the sketch. In figure 14, m* is a reference mass flow and is defined as the value corresponding to choking ($M = 1.0$) at the inlet throat area at free-stream total pressure. The experimental results presented in figure 14 agree closely with the theoretical results obtained for sharp-lip inlets at subsonic speeds as given in reference 4. Variations in angle of attack had little effect on the inlet performance. At sea level, the inlet would operate slightly subcritically and at a high pressure recovery when matched to the J67 engine. However, at an altitude of 35,000 feet, matching would occur in the inlet supercritical flow regime with a considerable loss in total-pressure recovery as indicated by the intersection of the match line with the performance curves.

The internal performance of one of the boundary-layer bleed ducts is presented in figure 15 for an angle of attack of 3.5° at free-stream Mach numbers of 2.0 and 1.8. At M_0 of 1.8, the bleed attained a higher supercritical mass-flow ratio and, at comparable corrected weight flows, a higher total-pressure recovery than at $M_0 = 2.0$. Variations in the boundary-layer mass flow had no apparent effect on the main inlet flow except when the duct was completely closed, as might have been expected from the results of reference 2. The

thrust-force coefficient of the bleed duct is defined as the change in momentum from the bleed inlet to the bleed exit. Therefore the thrust-force coefficient does not include the drag associated with the skin friction over the forward part of the body washed by the bleed mass flow, nor does it include the additive thrust term usually associated with duct flow and requiring the addition of the additive drag component. The thrust force, developed in the model by the action of the boundary-layer bleed plug, was inherent in the manner of testing, since, of course, in an actual installation the boundary-layer bleed duct without heat addition would produce only drag. The forebody-drag coefficient of the configuration includes this bleed-thrust force. However, for all the data presented, the boundary-layer-duct corrected weight flow per unit discharge area was held at 28.8 for M_0 of 2.0 and at 29.1 for M_0 of 1.8, where the internal force developed by the bleed system was approximately zero as shown in figure 15. Furthermore, at all operating conditions of the bleed duct, this force was quite small; for example, at the lowest duct corrected air flow investigated, the internal force coefficient developed by both ducts was only about 0.008, which is almost within the accuracy of the present drag measurements.

Figure 16 presents the variation of forebody efficiency for several variable-ramp angles at free-stream Mach numbers of 2.0, 1.8, and 1.5 at an angle of attack of 3.5°. This efficiency parameter is calculated by utilizing the ideal thrust $F_{n,id}$ of the J67-W-1 engine at an altitude of 35,000 feet. The expression $F_n/F_{n,id}$ is the ratio of actual to ideal thrust resulting from the loss in total-pressure recovery, and D is the over-all forebody drag. For $M_0 = 2.0$, the optimum variable-ramp angle is 17° because of higher matching total-pressure recovery and mass-flow ratio as shown in figure 7. However, figure 7 also indicates that at this variable-ramp angle the inlet has the least stable mass-flow range of the variable-ramp angles tested. For $M_0 = 1.8$, the same situation exists in that the match point for the optimum wedge angle of 14° occurs nearly at the minimum stable mass-flow point (fig. 8). For $M_0 = 1.5$, 10° was the optimum variable-ramp angle of two angles tested.

SUMMARY OF RESULTS

An investigation was conducted in the 8- by 6-foot supersonic tunnel to determine the performance of a twin-duct air-intake system mounted on the side of a supersonic airplane at Mach numbers 0.62 and from 1.5 to 2.0. The inlets had a double-oblique-shock system produced by a 10° precompression wedge and a variable-angle second ramp and were designed to supply air to a J67 engine. A previous investigation evaluated the performance of a similar air intake system mounted on the same

body but with fixed single-shock inlets designed for the J57 engine. The following results were obtained from the present investigation:

1. In contrast with the data of the previous investigation, dissimilar operation of the twin ducts occurred at the supersonic Mach numbers in that one duct operated critically or supercritically while the other operated subcritically.

2. The maximum stable subcritical range of about 13 percent was obtained at the highest ramp angles for Mach numbers of 1.8 and 2.0 and progressively decreased as the variable-ramp angle was decreased.

3229

3. Peak pressure recovery of 85 percent was obtained at Mach 2.0. The 15 percent loss from free-stream total pressure included a 4 percent total-pressure loss ahead of the inlet caused by the fuselage forebody. At Mach 0.62 good agreement was obtained between experimental and theoretical losses for sharp-lip inlets.

4. The variable-ramp inlet enabled the engine to be matched to the inlet at a high pressure recovery throughout the Mach number range. Subsonic matching at sea level occurred near critical inlet flow; however, at the higher altitudes the inlet matched supercritically.

Lewis Flight Propulsion Laboratory
National Advisory Committee for Aeronautics
Cleveland, Ohio, March 16, 1954

REFERENCES

1. Davids, Joseph, and Wise, George A.: Investigation at Mach Numbers 1.5 and 1.7 of Twin-Duct Side Intake System with Two-Dimensional 6° Compression Ramps Mounted on a Supersonic Airplane. NACA RM E53H19, 1953.

2. Obery, Leonard J., and Stitt, Leonard E.: Investigation at Mach Numbers 1.5 and 1.7 of Twin-Duct Side Air-Intake System with 9° Compression Ramp Including Modifications to Boundary-Layer-Removal Wedges and Effects of a Bypass System. NACA RM E53H04, 1953.

3. Bailey, Neil P.: The Thermodynamics of Air at High Velocities. Jour. Aero. Sci., vol. 11, no. 3, July 1944, pp. 227-238.

4. Fradenburg, Evan A., and Wyatt, DeMarquis D.: Theoretical Performance Characteristics of Sharp-Lip Inlets at Subsonic Speeds. NACA TN 3004, 1953.

[redacted]

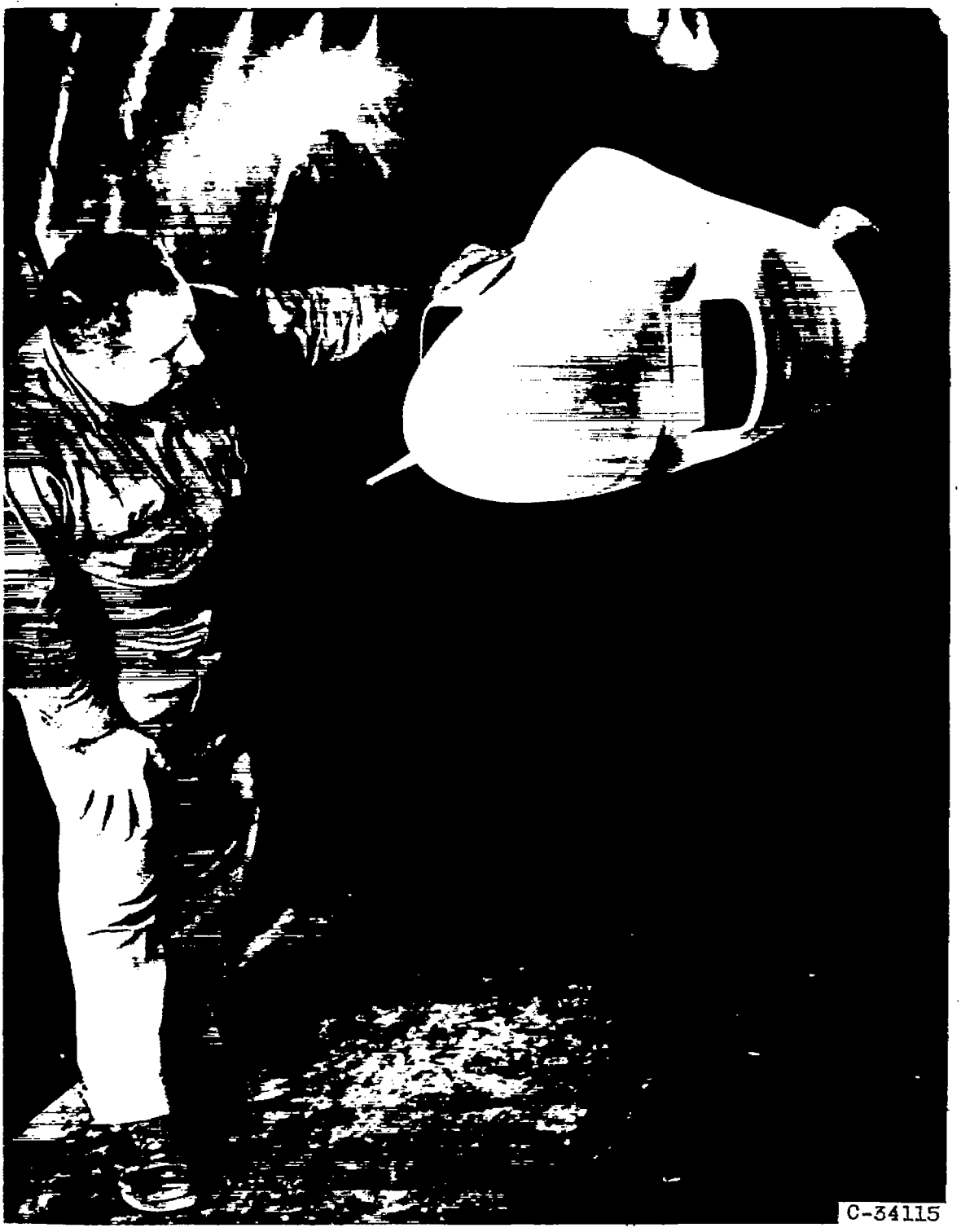

Figure 1. - Photograph of model.

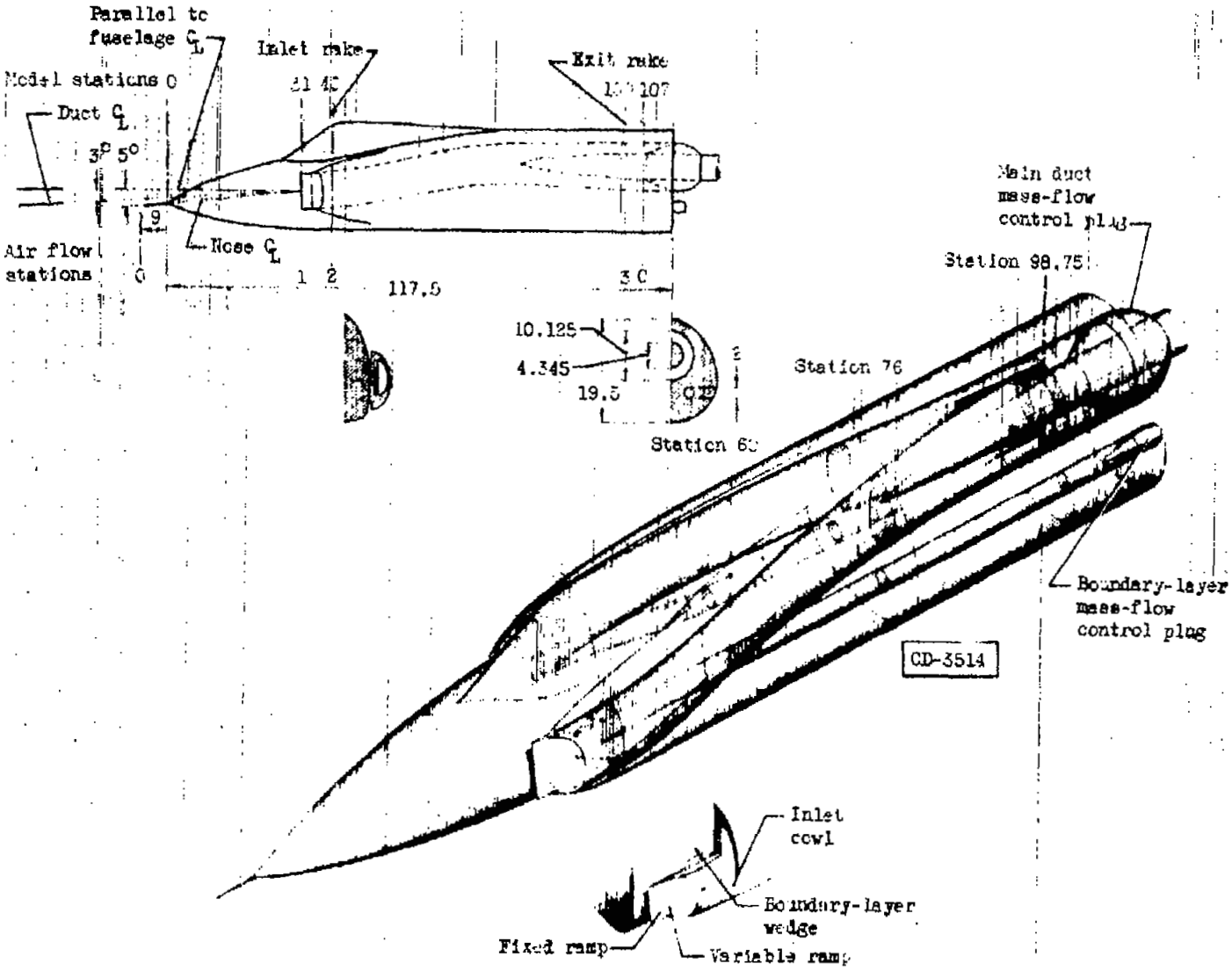

Figure 2. - Diagram of model with representative cross sections. (All dimensions are in inches.)

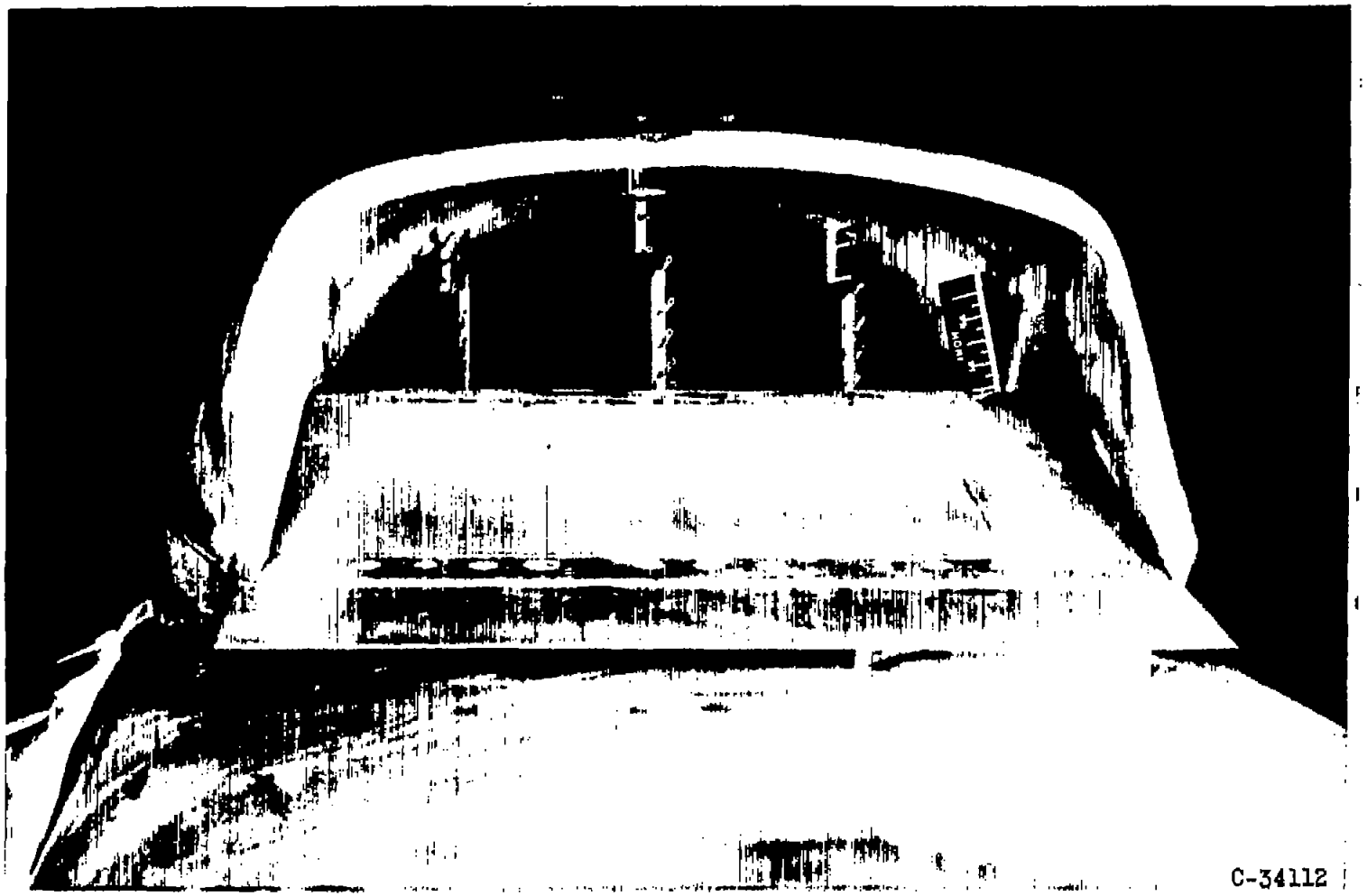

Figure 3. - Photograph of inlet.

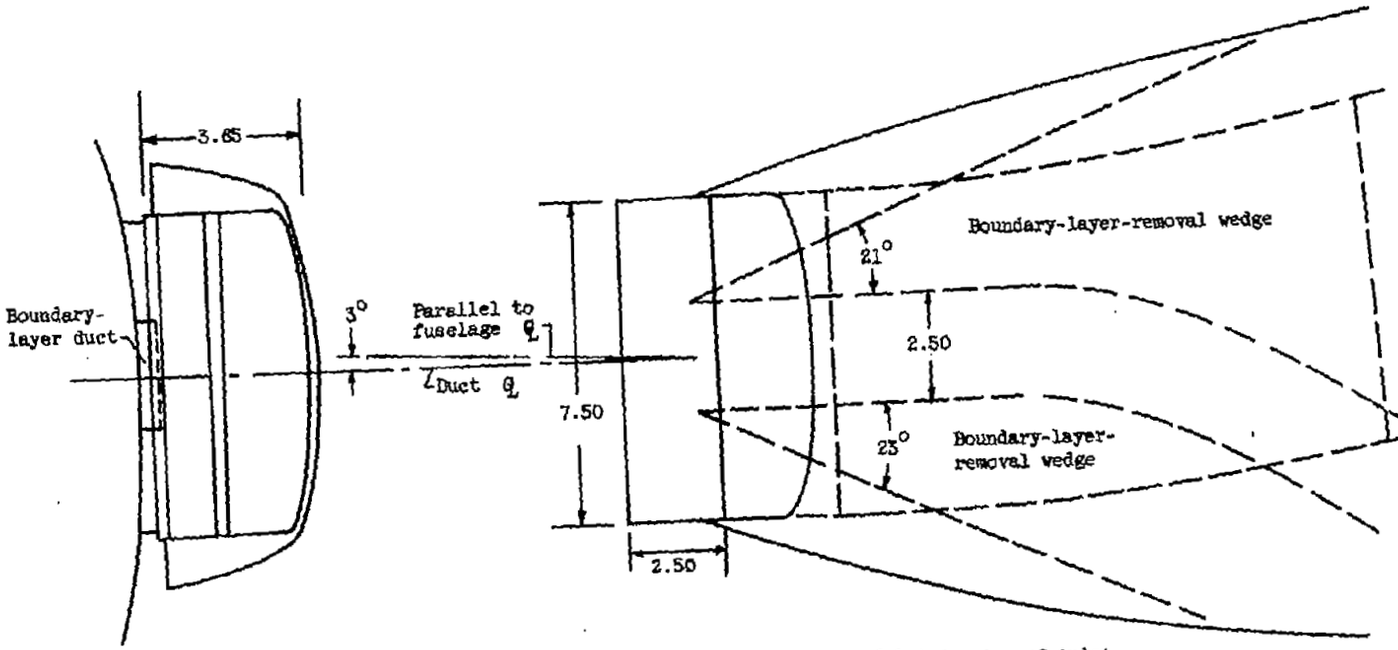

(a) Front view of inlet.

(b) Side view of inlet.

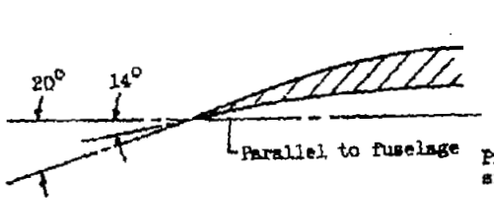

(d) Detail F.

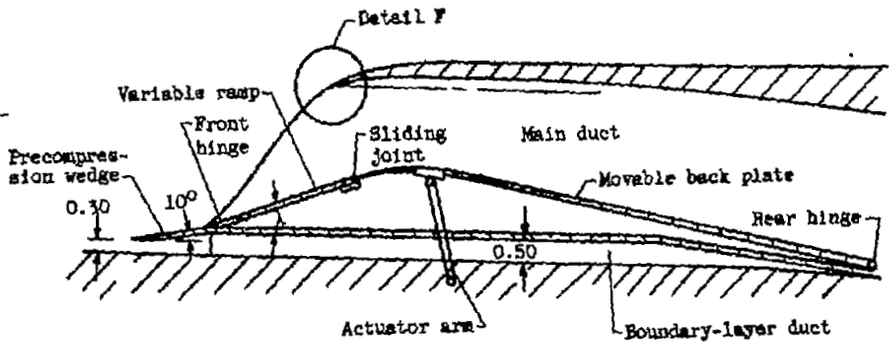

(c) View through duct center line.

Figure 4. - Detailed views of inlet configuration. (All dimensions are in inches.)

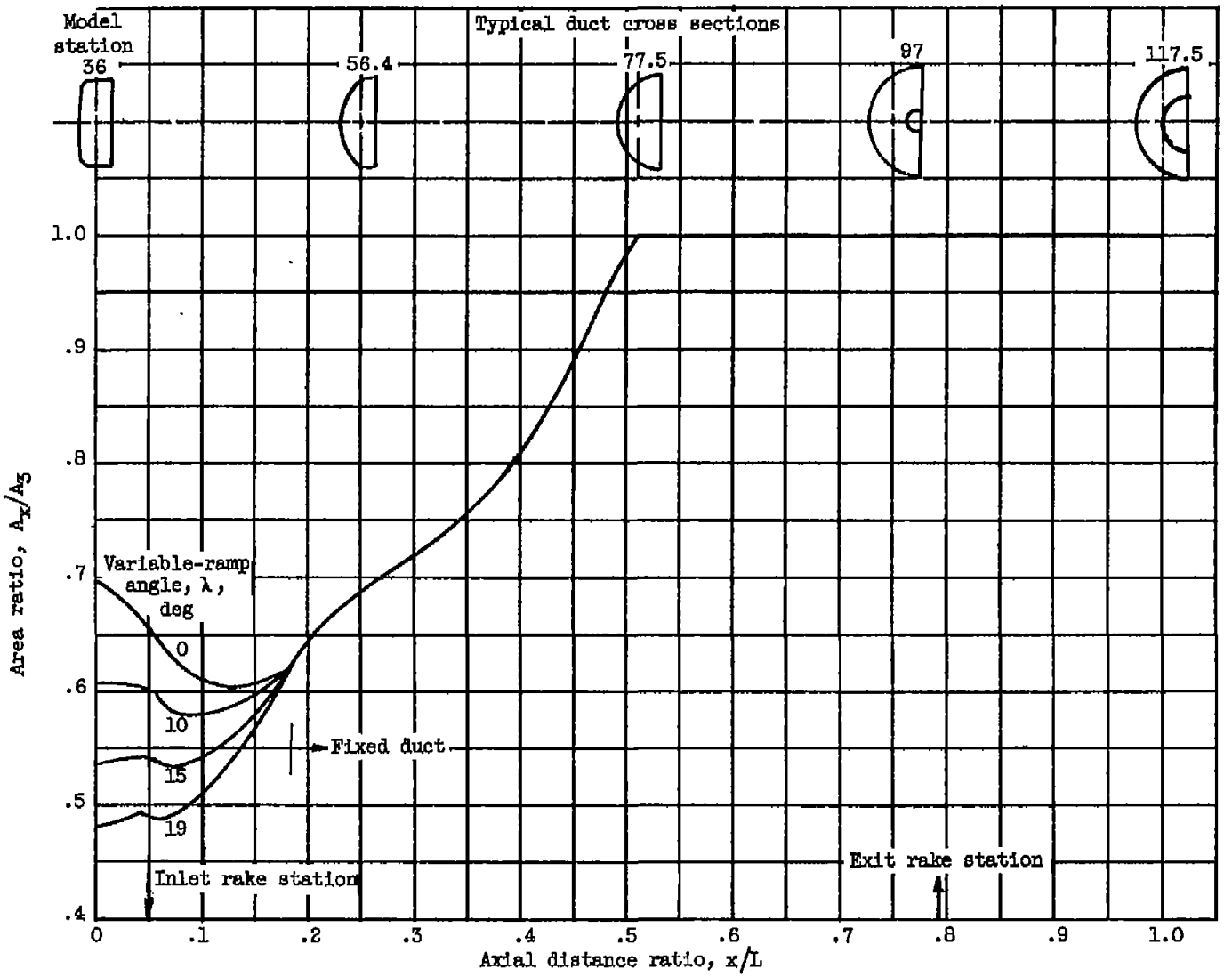

Figure 5.- Subsonic diffuser area variation. L, 81.5 inches; A_3, 0.457 square feet.

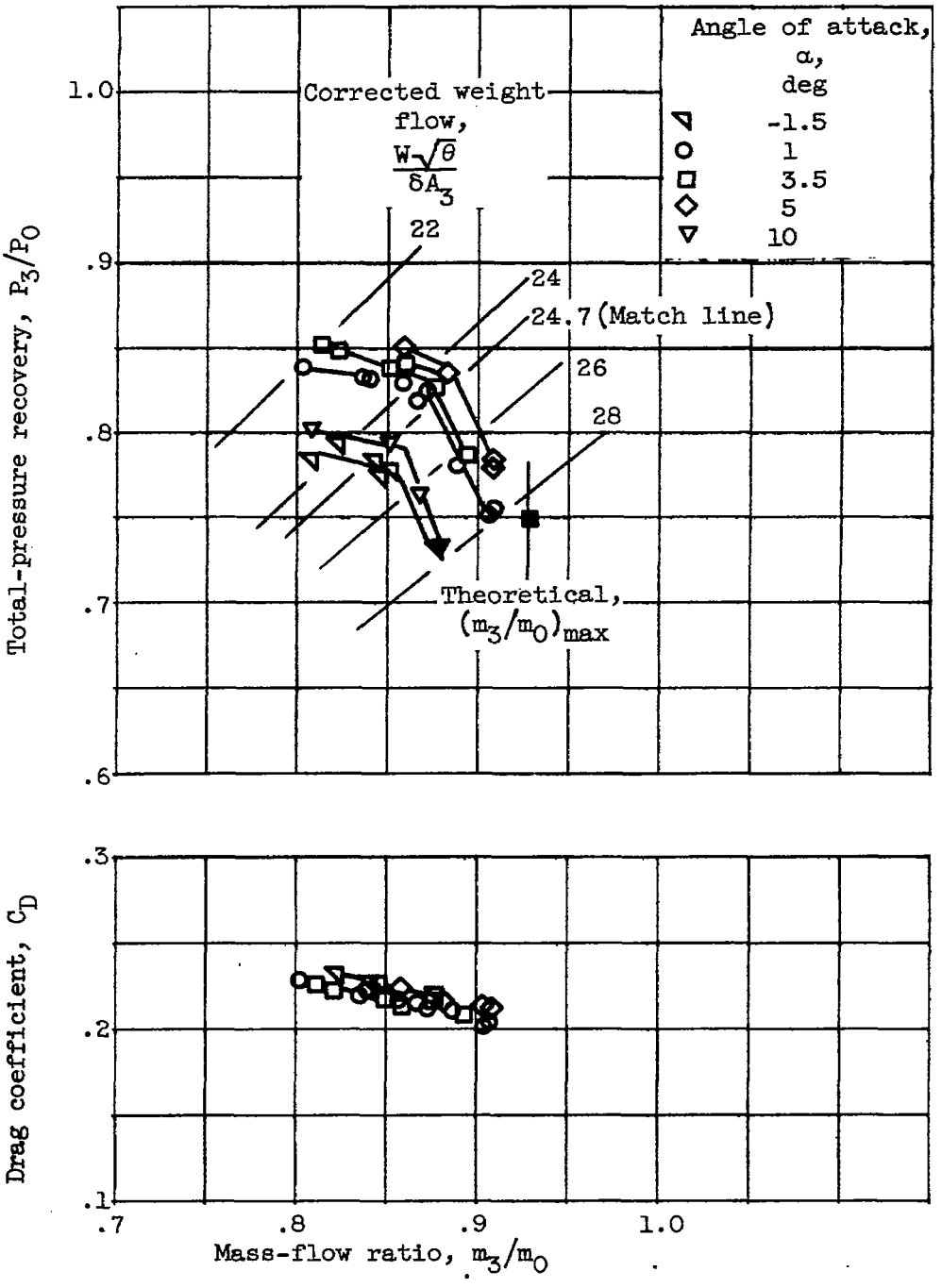

Figure 6. - Inlet performance characteristics at free-stream Mach number of 2.0 and variable-ramp angle of 19°.

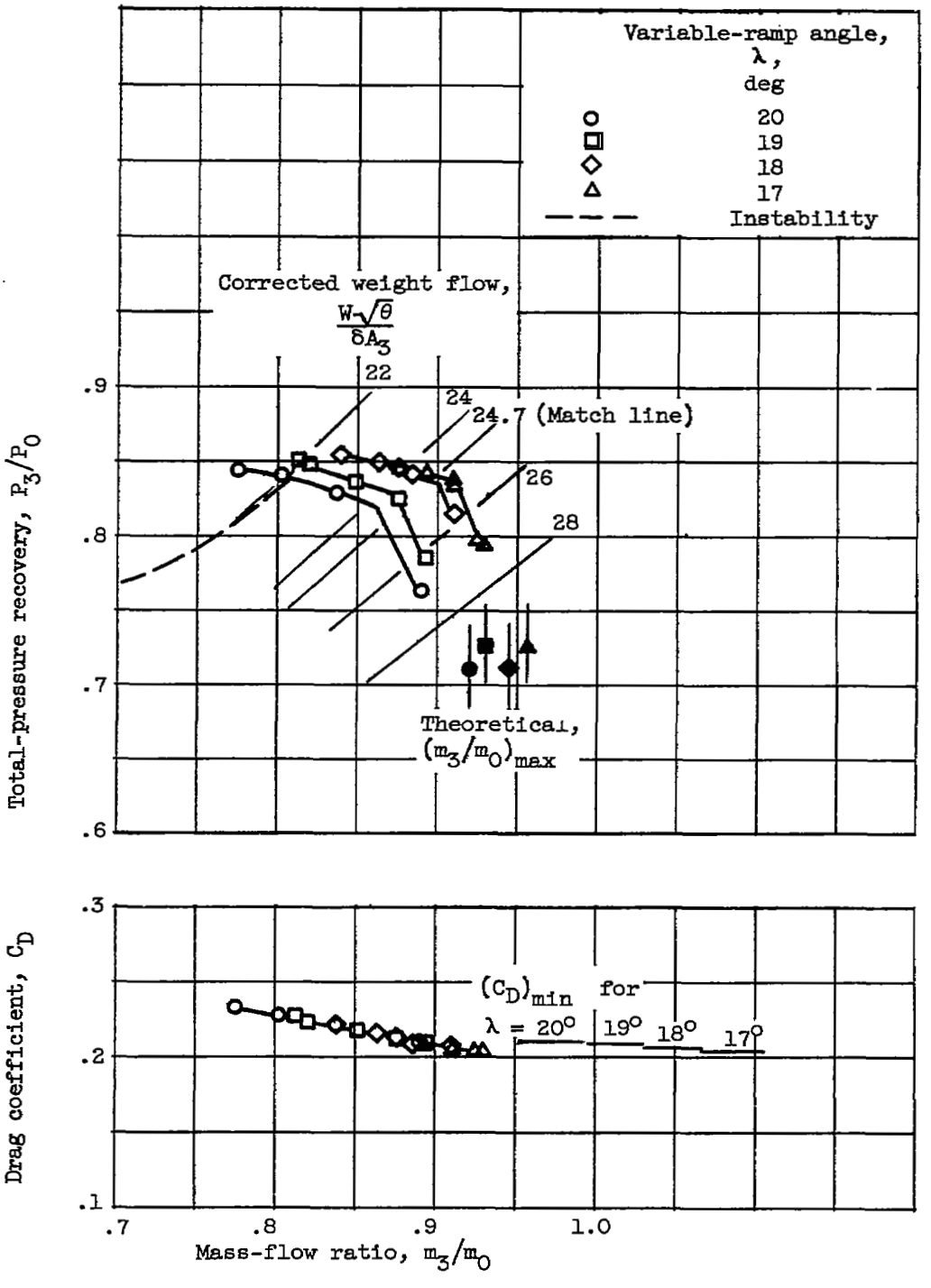

Figure 7. - Inlet performance characteristics at free-stream Mach number of 2.0 and angle of attack of 3.5°.

[redacted]

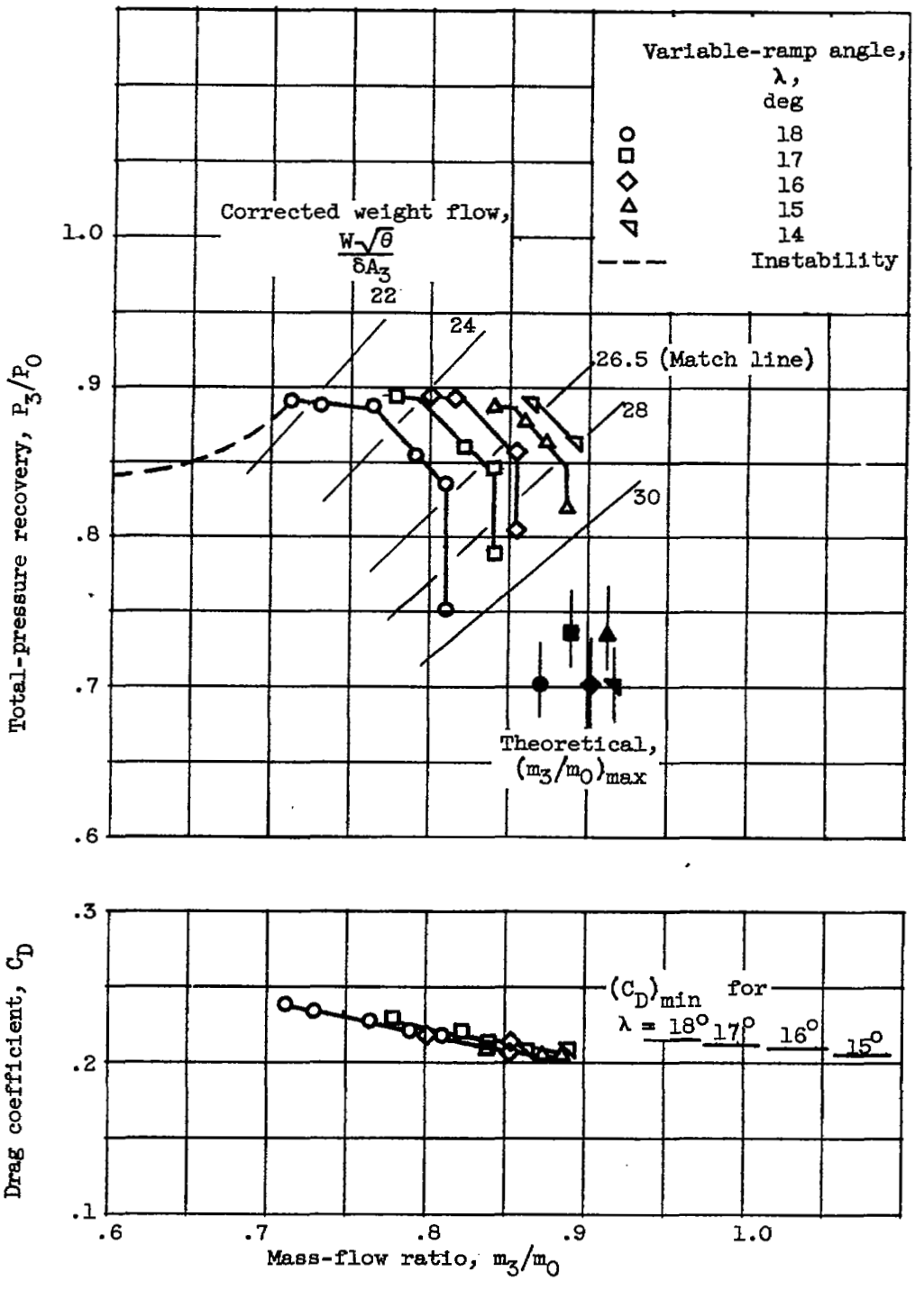

Figure 8. - Inlet performance characteristics at free-stream Mach number of 1.8 and angle of attack of 3.5°.

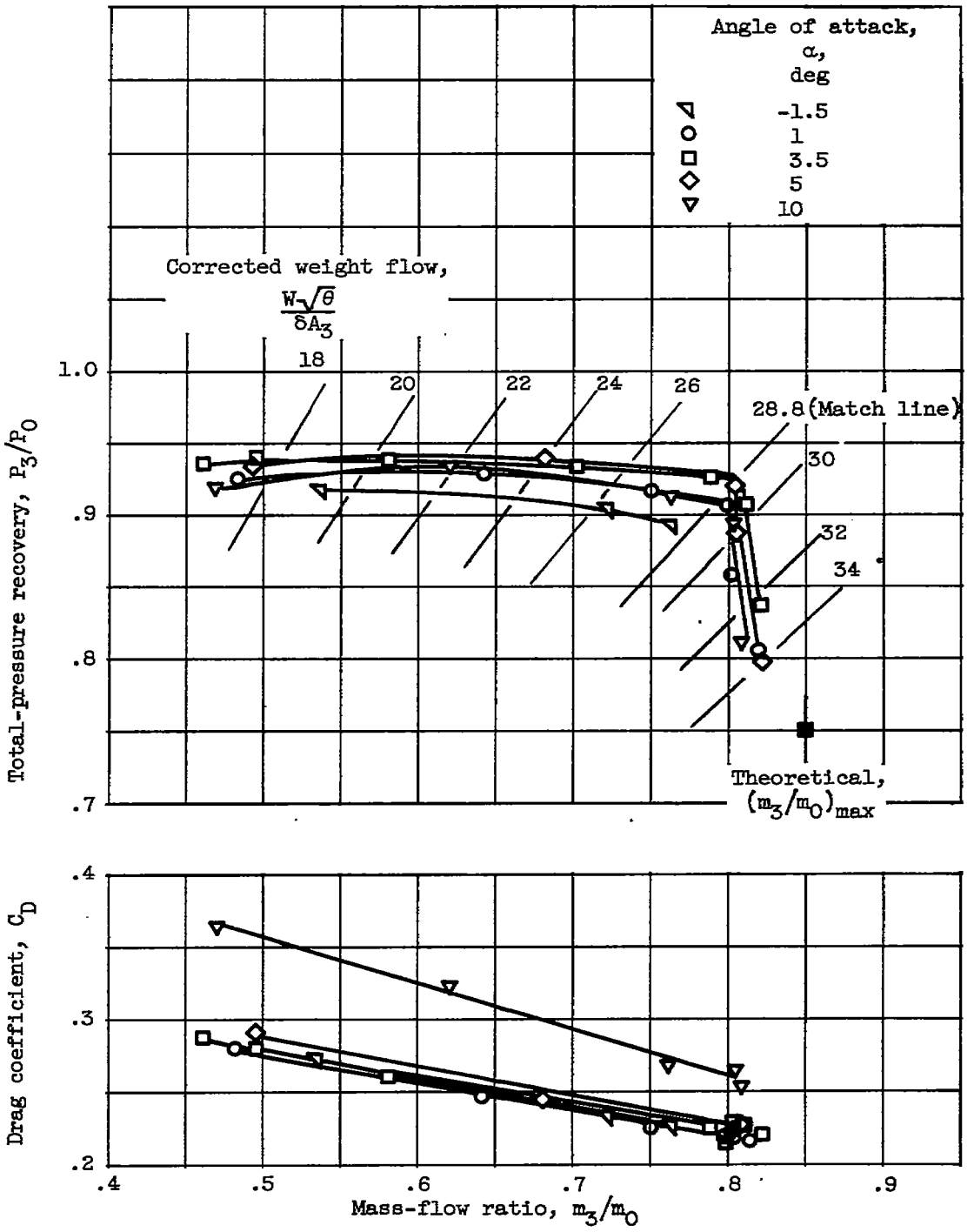

Figure 9. - Inlet performance characteristics at free-stream Mach number of 1.5 and variable-ramp angle of 10°.

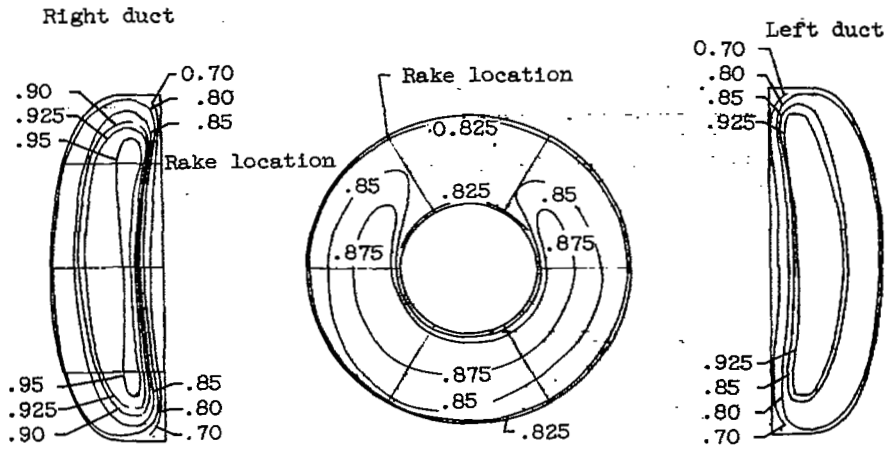

(a) Free-stream Mach number, 2.0; angle of attack, 3.5°; variable-ramp angle, 19°; mass-flow ratio, 0.813.

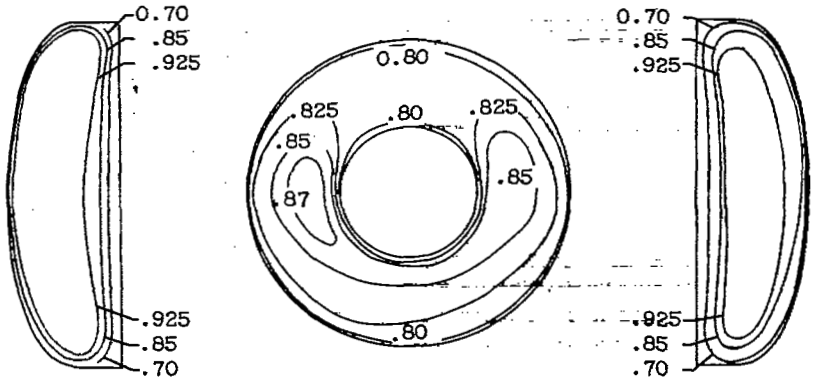

(b) Free-stream Mach number, 2.0; angle of attack, 3.5°; variable-ramp angle, 19°; mass-flow ratio, 0.876.

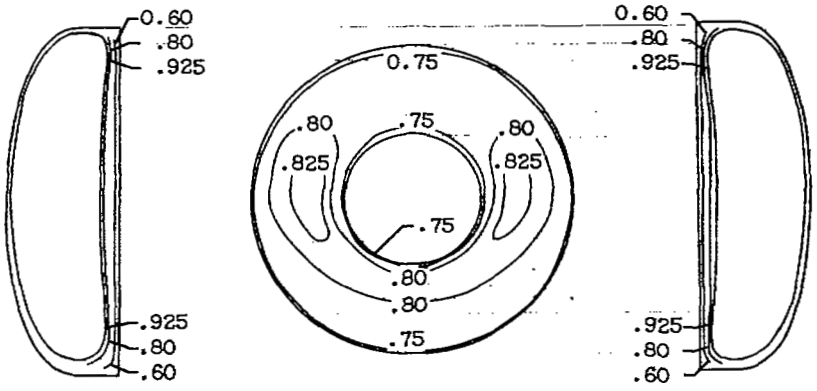

(c) Free-stream Mach number, 2.0; angle of attack, 3.5°; variable-ramp angle, 19°; mass-flow ratio, 0.894.

Figure 10. - Inlet and diffuser-exit total-pressure-recovery contours (view looking downstream).

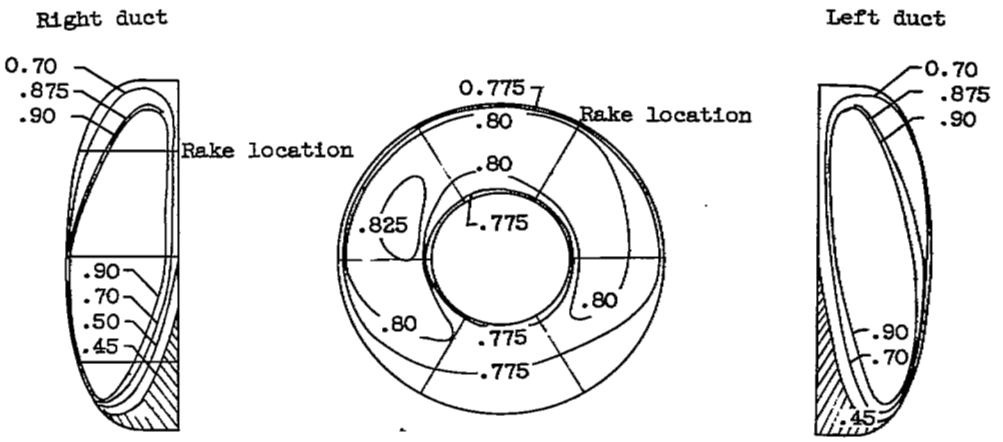

(d) Free-stream Mach number, 2.0; angle of attack, 10°; variable-ramp angle, 19°; mass-flow ratio, 0.867.

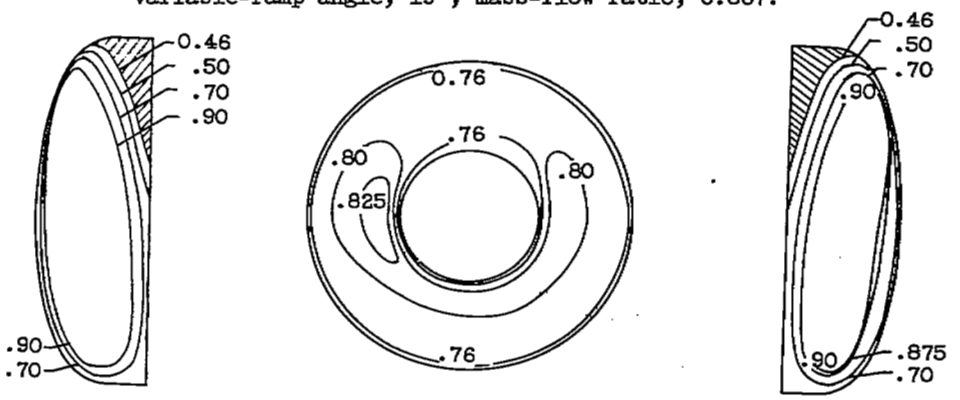

(e) Free-stream Mach number, 2.0; angle of attack, -1.5°; variable-ramp angle, 19°; mass-flow ratio, 0.854.

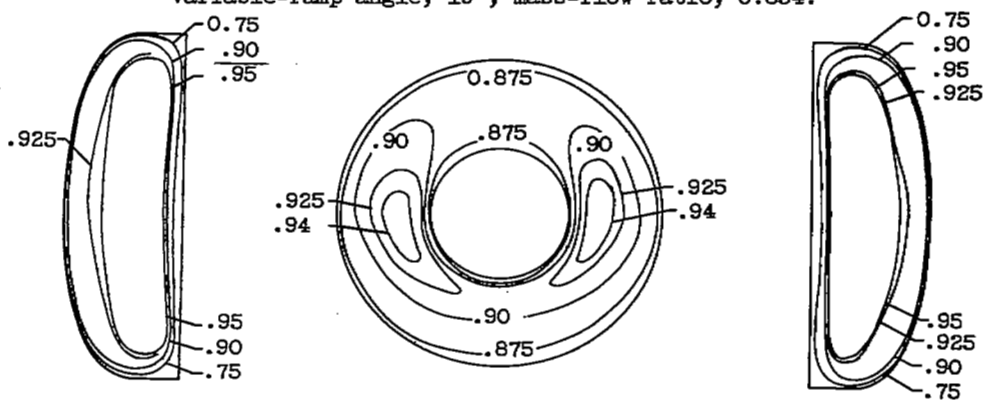

(f) Free-stream Mach number, 1.8; angle of attack, 3.5°; variable-ramp angle, 17°; mass-flow ratio, 0.777.

Figure 10. - Continued. Inlet and diffuser-exit total-pressure recovery contours (view looking downstream).

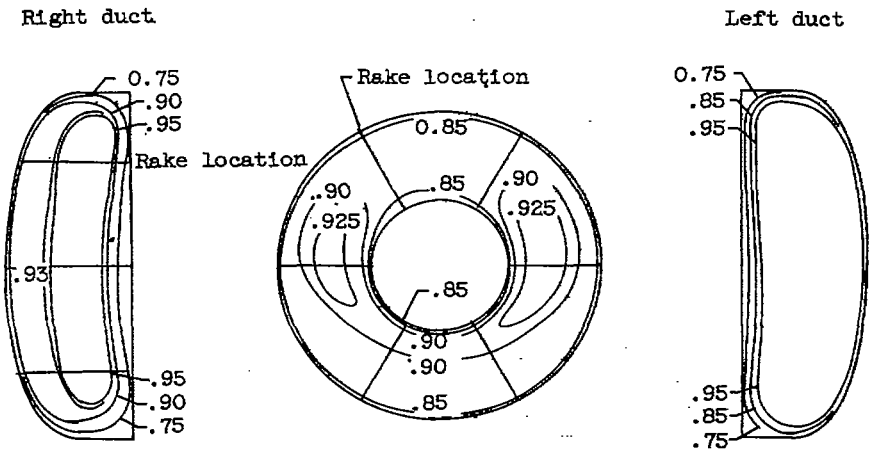

(g) Free-stream Mach number, 1.8; angle of attack, 3.5°; variable-ramp angle, 15°; mass-flow ratio, 0.865.

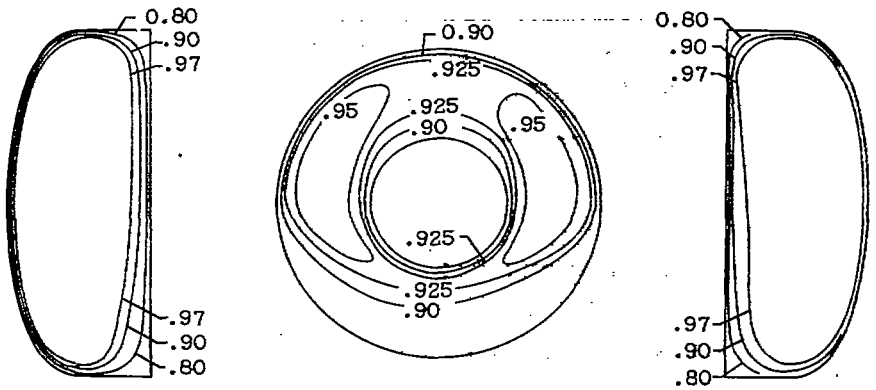

(h) Free-stream Mach number, 1.5; angle of attack, 3.5°; variable-ramp angle, 10°; mass-flow ratio, 0.786.

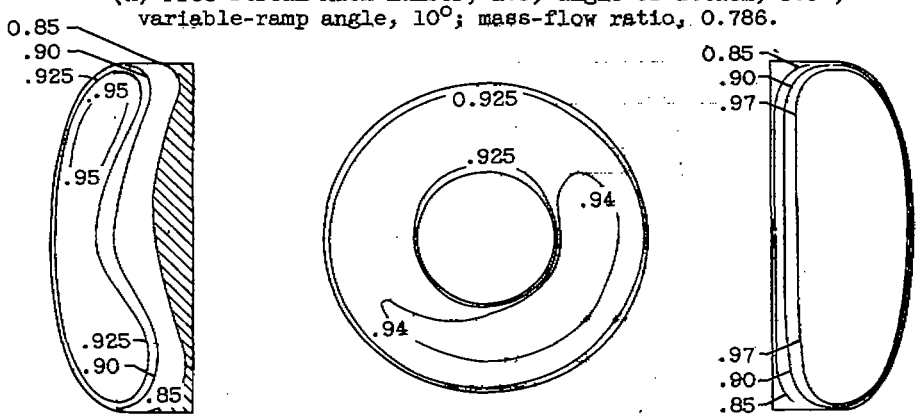

(i) Free-stream Mach number, 1.5; angle of attack, 3.5°; variable-ramp angle, 10°; mass-flow ratio, 0.495.

Figure 10. - Concluded. Inlet and diffuser-exit total-pressure-recovery contours (view looking downstream).

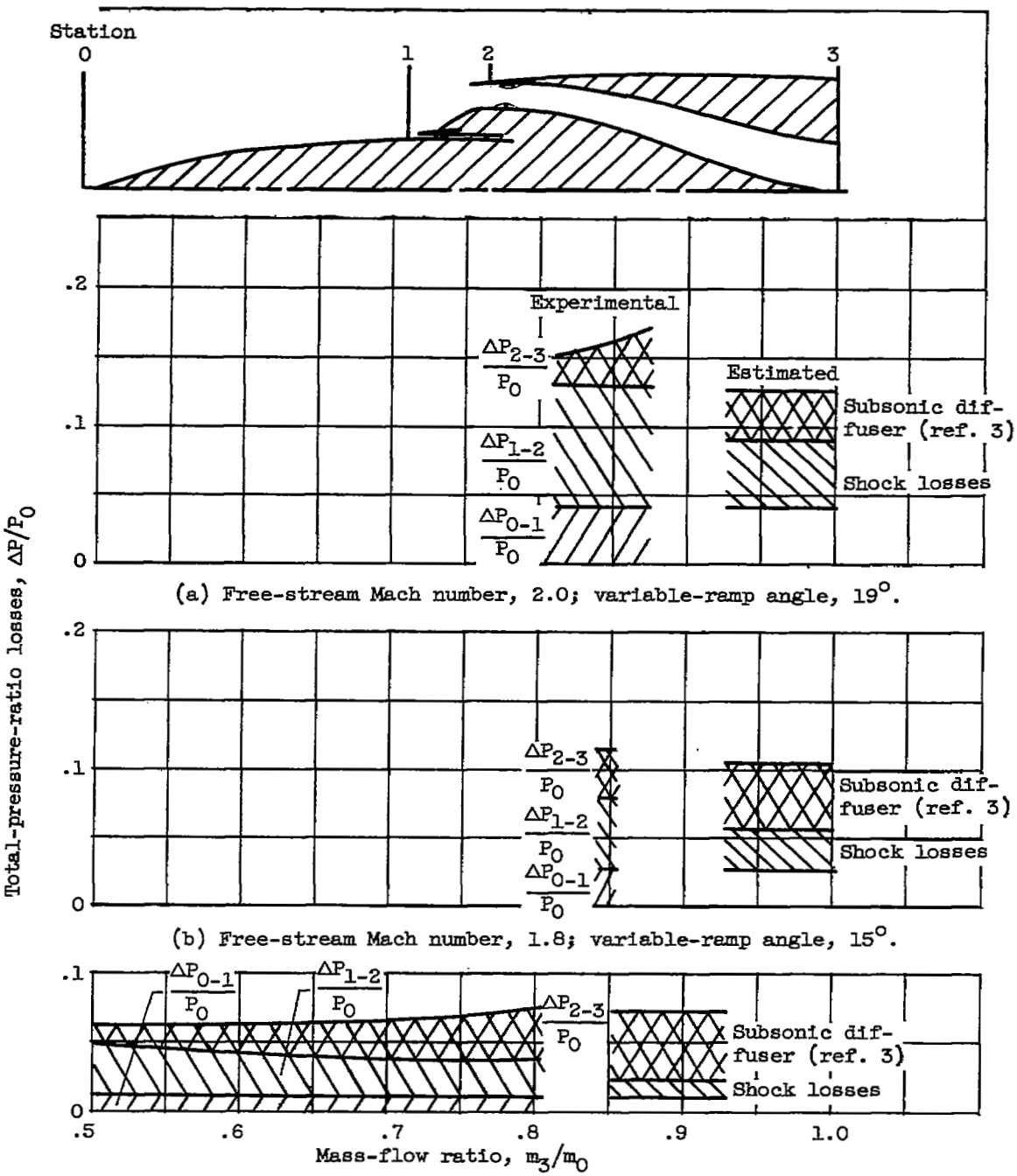

(a) Free-stream Mach number, 2.0; variable-ramp angle, 19°.

(b) Free-stream Mach number, 1.8; variable-ramp angle, 15°.

(c) Free-stream Mach number, 1.5; variable-ramp angle, 10°.

Figure 11. - Breakdown of total-pressure-ratio losses at angle of attack of 3.5°.

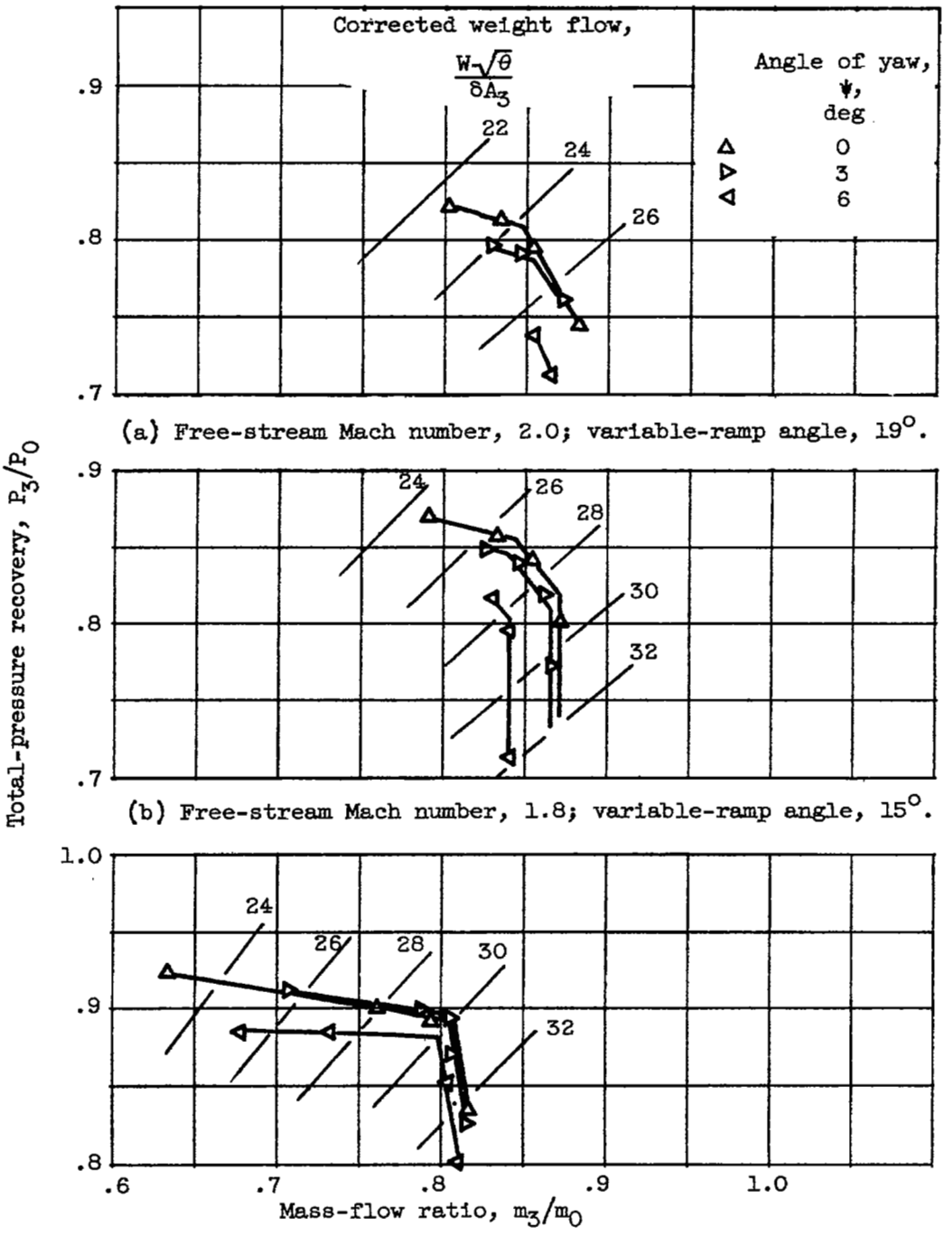

(a) Free-stream Mach number, 2.0; variable-ramp angle, 19°.

(b) Free-stream Mach number, 1.8; variable-ramp angle, 15°.

(c) Free-stream Mach number, 1.5; variable-ramp angle, 10°.

Figure 12. - Inlet performance characteristics.

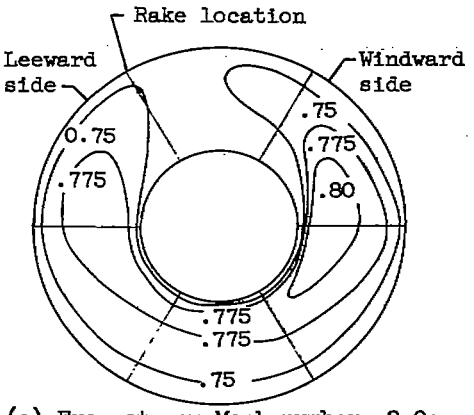

(a) Free-stream Mach number, 2.0; yaw angle, 3°; variable-ramp angle, 19°; mass-flow ratio, 0.871.

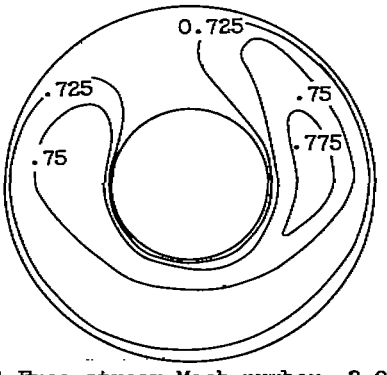

(b) Free-stream Mach number, 2.0; yaw angle, 6°; variable-ramp angle, 19°; mass-flow ratio, 0.854.

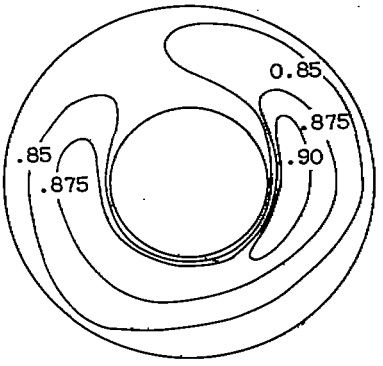

(c) Free-stream Mach number, 1.8; yaw angle, 3°; variable-ramp angle, 15°; mass-flow ratio, 0.825.

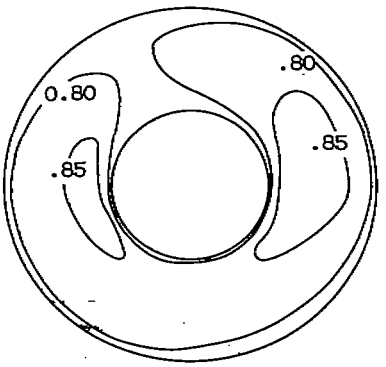

(d) Free-stream Mach number, 1.8; yaw angle, 6°; variable-ramp angle, 15°; mass-flow ratio, 0.839.

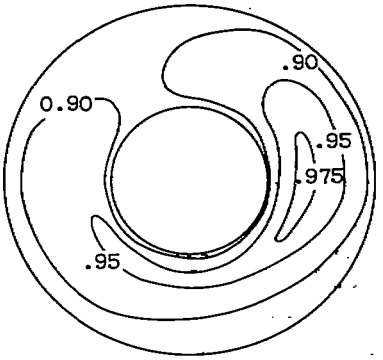

(e) Free-stream Mach number, 1.5; yaw angle, 3°; variable-ramp angle, 10°; mass-flow ratio, 0.712.

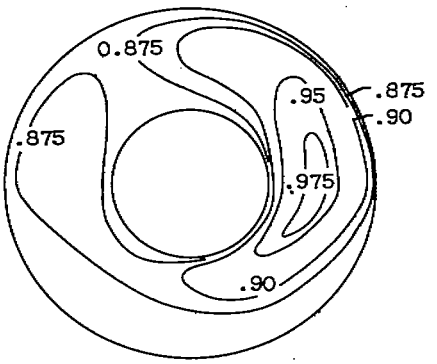

(f) Free-stream Mach number, 1.5; yaw angle, 6°; variable-ramp angle, 10°; mass-flow ratio, 0.677.

Figure 13. - Diffuser-exit total-pressure-recovery contours (view looking downstream).

[redacted]

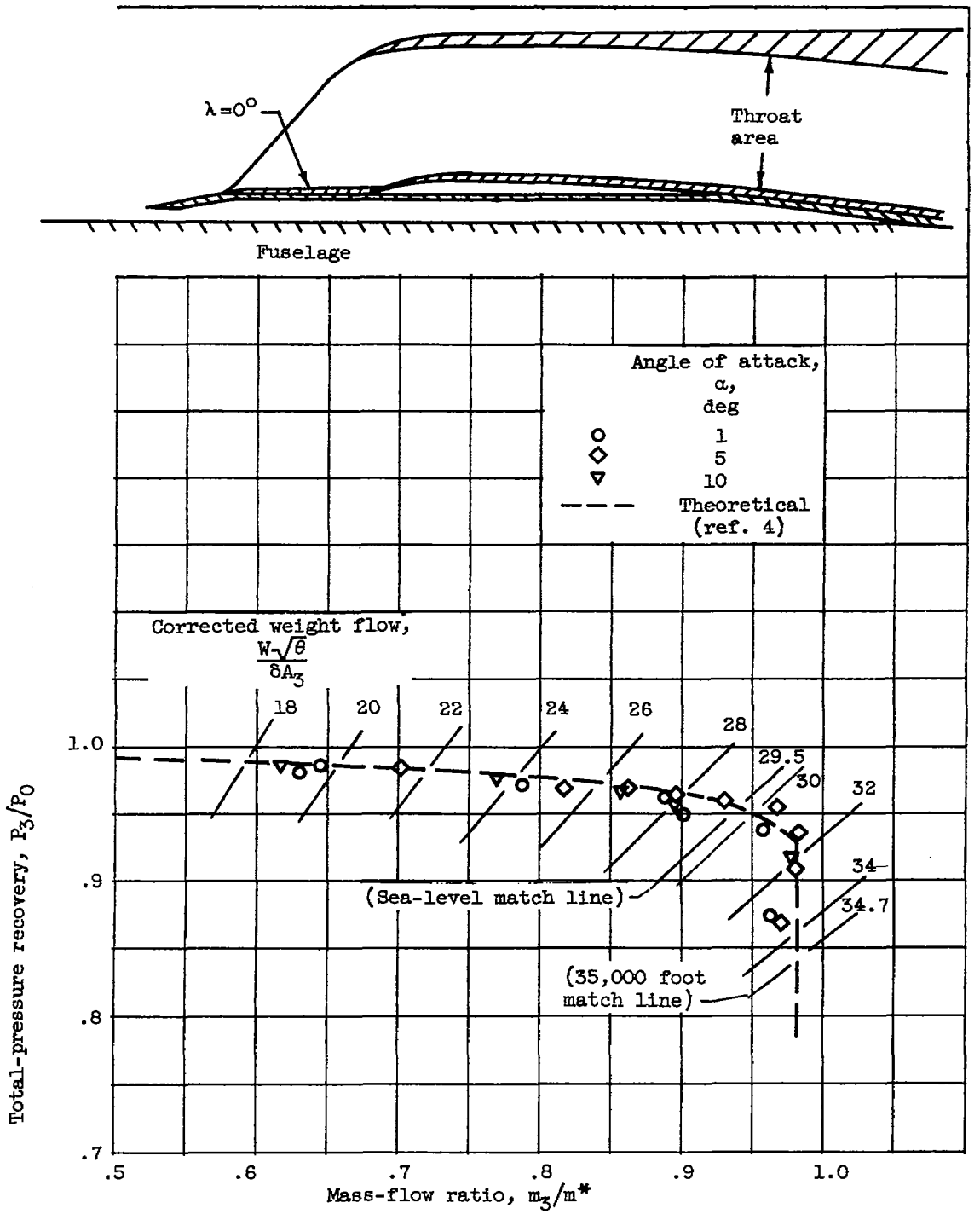

Figure 14. - Inlet performance characteristics at free-stream Mach number of 0.62 and variable-ramp angle of 0°.

[redacted]

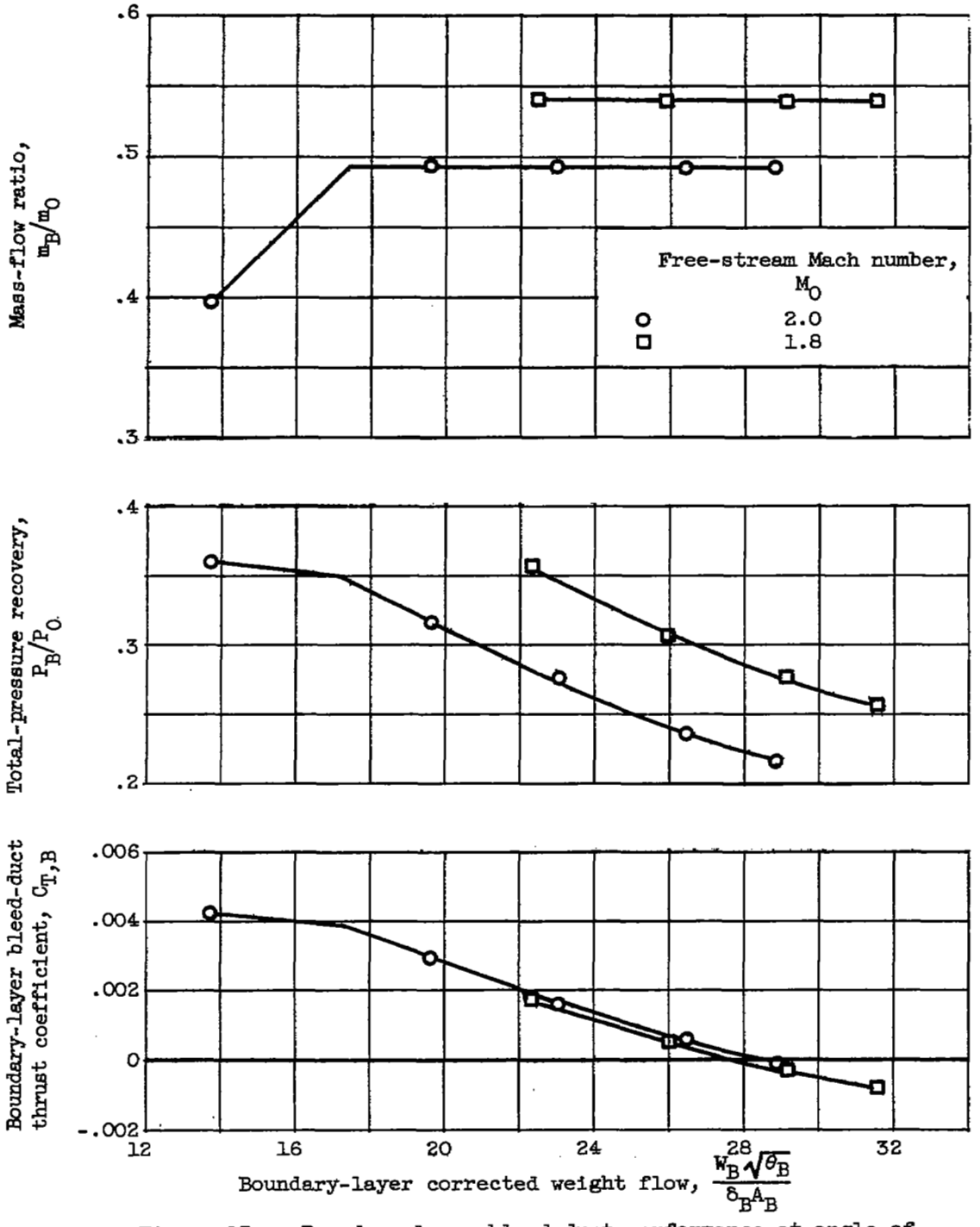

Figure 15. - Boundary-layer bleed-duct performance at angle of attack of 3.5°.

[redacted]

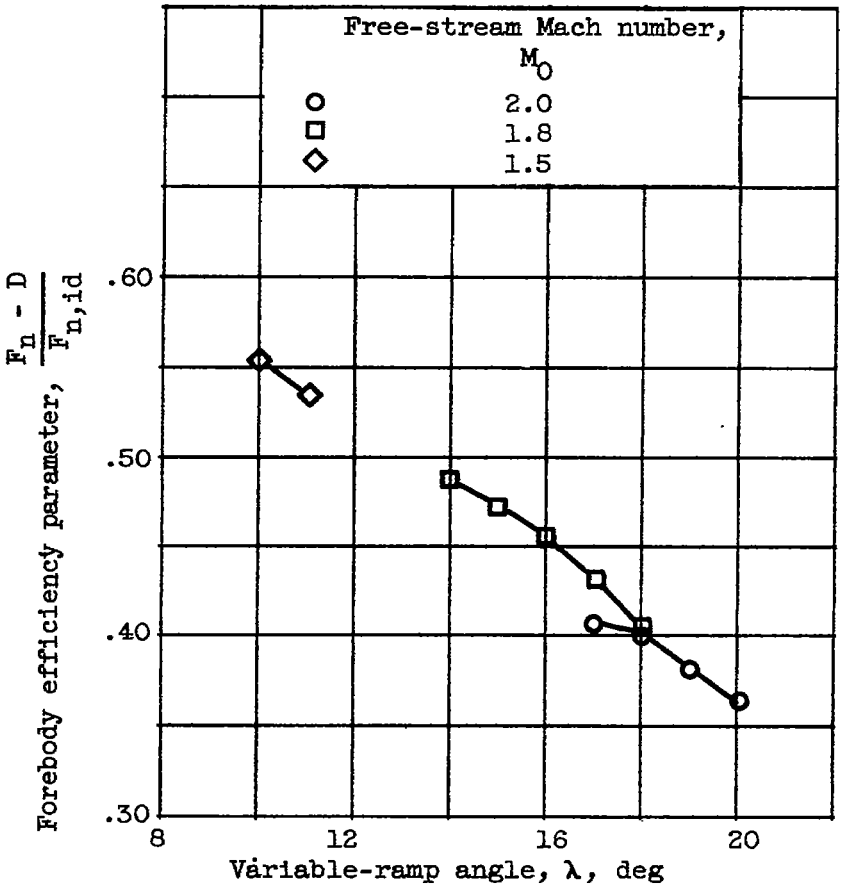

Figure 16. - Inlet efficiency based on J67-W-1 engine at angle of attack of 3.5° and altitude of 35,000 feet.

NACA-Langley - 8-19-54 - 350